Acta Mechanica Sinica (2015) 31(1):53–61
DOI 10.1007/s10409-015-0001-0

RESEARCH PAPER

A dynamic coupling numerical model for pollutant transport under wave condition

Yong Li · Mian Lin · Zhen Wang

Received: 13 May 2014 / Revised: 15 September 2014 / Accepted: 24 October 2014

Abstract In order to study the diffusion, migration, and distribution of pollutants among overlying water-body and porous seabed under wave conditions, a dynamic coupling numerical model is proposed. In this model, the coupling between wave field of overlying water-body and seepage of porous bed, the capture and release of pollutants in porous media, and the transport process between the two different regions are taken into account. We use the unified equations for pressure correction and pollutant concentration to solve the numerical model, which avoids repeated iteration on the interface boundary. The model is verified by several case studies. Afterwards, the processes involving release of pollutant from porous seabed and transportation to overlying water-body under different wave conditions are investigated. The results show that the water depth, wave height, and wave period have great influences on the release, capture, and transport processes for phosphorus pollutant.

Keywords Wave · Pollutant · Transport process · Dynamic coupling model · Numerical analysis

1 Introduction

During the past several decades, a lot of domestic and industrial sewage has been drained into seawater, and thus coastal environment has been seriously destroyed. The pollutant transport process is much complicated by the complicated hydrodynamics in coastal zones. The captured pollutant in porous seabed can be released under certain wave conditions, increasing the concentration of pollutant in overlying water-body, which is called secondary pollution. It is important to analyze pollutant transport between the bottom porous media and the overlying water-body.

Modeling pollutant transport process in coastal zones has long been a subject of research for hydraulic and environmental engineers. Much progress on numerical modeling has been made. Falconer [1] used a hydrodynamic water quality model to predict the depth mean nitrogen concentrations in nature harbor. Mestres [2] solved the three-dimensional advection-diffusion equation by using random walk Lagrangian particle formulation. Pollutant transport induced by currents, waves, and turbulent diffusion was considered in the model calculations. Tao and Han [3] studied the effects of water wave motion on pollutant transport in shallow coastal water. Numerical simulation shows that the pollutant will transfer along shore when the incident wave is at an angle to the shoreline. Sun and Tao [4] built a numerical model of pollutant transport acted by water waves. The numerical model was combined with a wave propagation model, a multiple wave-breaking model, a wave-induced current model, and a pollutant convection–dispersion model. Tang et al. [5] got the variation curve of the longitudinal dispersion coefficient versus non-dimensional wave height and water depth by numerical simulation of pollutant transport. Tang and Cui [6] investigated the pollutant transport in breaking random water waves on mild slope zone. In their models, the propagation of random water waves was modeled by parabolic mild slope equation, the breaking random wave induced currents were modeled by shallow water equation, and the pollutant transport in surf zone was modeled by pollutant motion model. However, the porous bed is ignored in these studies, and the models can not be used to study the release of pollutant caused by wave motions and do not include the effect of pore scale properties of porous media on the pollutant transport and exchange. Amendment of the

The project was supported by the National Natural Science Foundation of China (11032007) and the Key Instrument Developing Project of the CAS (ZDYZ2012-1-08-02).

Y. Li · M. Lin (✉) · Z. Wang
Institute of Mechanics, Chinese Academy of Sciences,
100190 Beijing, China
e-mail: linmian@imech.ac.cn

model is crucial to improve the understanding of pollutant transport under wave conditions.

In the present study, a dynamic coupling numerical model is proposed. In this model, the wave field of overlying water-body is coupled with seepage of porous sea bed, and the pollutant can dynamically transport between the two different regions. In addition, the capture and release of pollutant in porous bed is also carefully modeled at a fine level. The model is verified and used to investigate the pollutant transport under different wave conditions.

2 Model formulation

2.1 Overlying water-body

The governing equations for overlying water-body are the RANS equations, which can be written as follows

$$\frac{\partial u_j}{\partial x_j} = 0, \tag{1}$$

$$\frac{\partial u_i}{\partial t} + \frac{\partial u_j u_i}{\partial x_j} = -\frac{1}{\rho}\frac{\partial p}{\partial x_i} + \frac{1}{\rho}\frac{\partial}{\partial x_j}\left[\mu_{\text{eff}}\left(\frac{\partial u_j}{\partial x_i} + \frac{\partial u_i}{\partial x_j}\right)\right] - D_i u_i + g_i, \tag{2}$$

where x_j ($j = 1, 2$) represents the coordinate component, u_i is the fluid velocity, p is the pressure, ρ is the density, g_i is the acceleration of gravity, D_i is the damping coefficient and the damping term $D_i u_i$ is added to the momentum equation directly. $\mu_{\text{eff}} = \mu + \mu_f$, μ is the molecular viscosity, μ_f is the turbulent eddy viscosity, $\mu_f = C_\mu \rho k^2/\varepsilon$. k is the turbulent kinetic energy, ε is the turbulent energy dissipation rate. Cheng et al. [7] proposed a new coupling model of wave interaction with porous medium. The model is established based on the RANS equations and the k–ε two-equation model. Similar work can also be found in Hsu et al. [8]. In the present paper, the RNG k–ε two-equation model is adopted to estimate the turbulence

$$\frac{\partial \rho k}{\partial t} + \frac{\partial \rho u_j k}{\partial x_j} = \frac{\partial}{\partial x_j}\left(\alpha_k \mu_{\text{eff}} \frac{\partial k}{\partial x_j}\right) + P_k - \rho\varepsilon, \tag{3}$$

$$\frac{\partial \rho \varepsilon}{\partial t} + \frac{\partial \rho u_j \varepsilon}{\partial x_j} = \frac{\partial}{\partial x_j}\left(\alpha_\varepsilon \mu_{\text{eff}} \frac{\partial \varepsilon}{\partial x_j}\right) + C^*_{1\varepsilon} P_k \frac{\varepsilon}{k} - \rho C_{2\varepsilon}\frac{\varepsilon^2}{k}, \tag{4}$$

where $P_k = \mu_f\left(\frac{\partial u_i}{\partial x_j} + \frac{\partial u_j}{\partial x_i}\right)\frac{\partial u_i}{\partial x_j}$, $C^*_{1\varepsilon} = C_{1\varepsilon} - \frac{\eta(1-\eta/\eta_0)}{1+\beta\eta^3}$, $\eta = (2S_{ij}S_{ij})^{0.5}\frac{k}{\varepsilon}$, $S_{ij} = \frac{1}{2}\left(\frac{\partial u_i}{\partial x_j} + \frac{\partial u_j}{\partial x_i}\right)$. The values of constants in RNG k–ε model are given in Table 1.

Table 1 The values of constants in turbulent model

Constant	C_μ	α_k	α_ε	$C_{1\varepsilon}$	$C_{2\varepsilon}$	η_0	β
Value	0.084 5	1.39	1.39	1.42	1.68	4.38	0.012

In order to capture the water–air free surface, an Eulerian method, named as the volume of fluid (VOF) method, is adopted and the size of air domain for the y direction is equal to the wave height. The equation for the volume fraction is

$$\frac{\partial \alpha}{\partial t} + \frac{\partial u_j \alpha}{\partial x_j} = 0, \tag{5}$$

where α is the volume fraction of water and $1 - \alpha$ represents the volume fraction of air. Volume fraction of each fluid is used as the weighting factor to get the mixture properties, for the density and molecule viscosity

$$\rho = \alpha\rho_{\text{w}} + (1-\alpha)\rho_{\text{a}}, \tag{6}$$

where ρ_{w} and ρ_{a} represent the density of water and air, respectively.

2.2 Porous media

Cheng et al. [7] indicated that the porous flow inside the porous media is within a transition region from laminar to turbulent flow and can be simulated by employing the Forcheimer's equation. For high velocities in porous media under wave action, inertial effects may well become significant. The Forcheheimer equation considers the effects, which can be expressed as

$$(1 + c_m)\frac{\partial u_i}{\partial t} + b\left|u_{jj}\right| u_i = g_i - \frac{1}{\rho}\frac{\partial p}{\partial x_i} - a u_i, \tag{7}$$

where p represents pore pressure, u_i is the pore velocity and c_m is the additional mass coefficient. Up to present, the reasonable value of c_m has been not clear. Zang [9] indicated that the value of c_m has very little impact on the results. In the present study, the value of additional mass coefficient is set to zero. The values of a and b can be obtained by the Van Gent formula [10]

$$a = a_0 \frac{\nu(1-\varphi)^2}{\varphi^3 D_{50}^2}, \tag{8}$$

$$b = \beta_0\left(1 + \frac{7.5}{KC}\right)\frac{(1-\varphi)}{\varphi^3 D_{50}}, \tag{9}$$

where φ is porosity, $a_0 = 1\,000$, $\beta_0 = 1.1$. ν is kinematic viscosity coefficient. KC is Keulegan–Carpenter number, which represents the ratio of characteristic lengths of fluid particle and porous media, $KC = U_{\max} T/(\varphi D_{50})$, where $U_{\max}$is maximum velocity near interface, T is wave period, D_{50} is characteristic diameter of porous media.

2.3 Pollutant transport

Simulation of pollutant transport is based on advection-dispersion equation. In overlying water body, transport equation of particle is as follows

$$\frac{\partial C}{\partial t} = \frac{\partial}{\partial x_i}\left(D^m_{ij}\frac{\partial C}{\partial x_j}\right) - v_j\frac{\partial C}{\partial x_j}. \tag{10}$$

Transport equation of pollutant in porous sea bed is

$$\frac{\partial C}{\partial t} = \frac{\partial}{\partial x_i}\left(D^h_{ij}\frac{\partial C}{\partial x_j}\right) - v_j\frac{\partial C}{\partial x_j} - \frac{\partial S}{\partial t}, \tag{11}$$

$$\frac{\partial S}{\partial t} = k_{\text{c}} C - k_{\text{r}} S, \tag{12}$$

where C is concentration of suspended pollutant, S is concentration of pollutant absorbed by pore wall. D_{ij}^m is molecular diffusion coefficient. D_{ij}^h is pollutant diffusion coefficient. v_j is the particle velocity, which takes the same value as fluid velocity in porous media. k_c and k_r are capture rate and release rate, respectively.

In the above equations, the capture and release of pollutant are considered. In this regard, Compere et al. [11] found that the first-order rate equation (Eq. (12)) can be used to simulate the release and capture processes of pollutant particle.

The discrete form of Eq. (12) can be written as

$$\frac{\Delta S}{\Delta t} = \frac{\Delta S_c - \Delta S_r}{\Delta t} = k_c C - k_r S. \tag{13}$$

Further, k_c and k_r can be expressed as

$$k_c = \frac{\Delta S_c}{C \Delta t}, \tag{14}$$

$$k_r = \frac{\Delta S_r}{S \Delta t}, \tag{15}$$

where, ΔS_c and ΔS_r are the concentration change of S in time interval Δt due to the capture and release of the pollutant respectively. S_c, S_r, C, and S can be obtained by the pore network mode, see e.g. Refs. [12, 13].

2.4 Boundary and initial conditions

The entire study domain is shown in Fig. 1. There are totally four types of boundaries, including inlet, outlet, porous bed, and atmosphere.

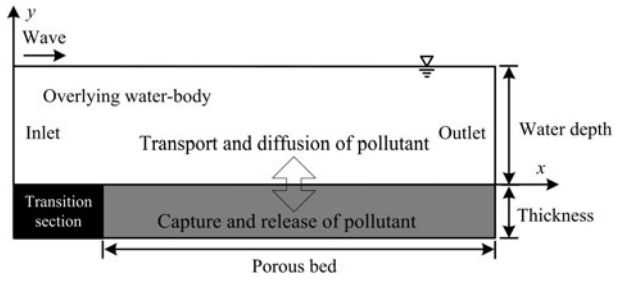

Fig. 1 Sketch of the computational domain

Boundary conditions associated with regular waves are prescribed along the inlet boundary. The velocity vector of regular wave is specified by the Stokes wave. The theoretical velocity of second-order Stokes wave can be expressed as

$$u_x^m = \frac{agH}{2\omega}\frac{\cosh[a(z+d)]}{\cosh(ad)}\cos(ax-\omega t) + \frac{3\omega a H^2}{16}\frac{\cosh[2a(z+d)]}{\sinh^4(ad)}\cos[2(ax-\omega t)], \tag{16}$$

$$u_y^m = \frac{agH}{2\omega}\frac{\sinh[a(z+d)]}{\cosh(ad)}\sin(ax-\omega t) + \frac{3\omega a H^2}{16}\frac{\sinh[2a(z+d)]}{\sinh^4(ad)}\cos[2(ax-\omega t)], \tag{17}$$

where H, ω, a, and d are wave height, frequency, wave number, and water depth, respectively. Here $\omega = 2\pi/T$, $a = 2\pi/L$, L is the wave length. x is the distance from the origin to the wave-making point.

At the outlet, non-reflective boundary condition combines damping zone and the radiation boundary condition. The velocity is specified by Sommerfeld radiation condition (SRC), expressed by

$$\frac{\partial u}{\partial x} + \frac{1}{c}\frac{\partial u}{\partial t} = 0, \tag{18}$$

where c is the wave propagation velocity at the end point of damping zone. As for the damping zone, $D_i u_i$ damping term is added to the momentum equation, showed as Eq. (2) and D_i is expressed as

$$D_i = \theta_i \sqrt{\frac{g}{d}}(n+1)\left(\frac{x-x_0}{l}\right)^n, \tag{19}$$

where x_0 is distance from the origin to the starting point of damping zone. n and θ_i are the damping coefficients, $n = 2$, $\theta_i = 0.6$.

As for the porous bed boundary, free slip boundary and wall functions are used. At the atmosphere boundary, the total pressure is set to zero. It is noted that there is no boundary condition needed at the interface between the porous flow and the overlying wave field by using a highly efficient coupling method. Cheng et al. [7] introduced a velocity–pressure correction equation for the waves and porous flow. The two flows are solved simultaneously. The continuity equation is enforced implicitly to ensure that the velocity and pressure of the two flows on the interface remain equal. The concentration boundary condition for interface is also not required because of solving the unified equation (Eq. (11)).

The black region at the lower left corner in Fig. 1 represents the non-permeable bed. The length of this transition region is twice the wave length. Free slip boundary and wall functions are also employed on these bed boundaries.

3 Numerical implementation

The Navier–Stokes (N–S) equations are discretized based on the finite volume method (FVM). The preconditioning conjugate gradient (PCG) method is employed to solve the algebraic equations. The pressure implicit splitting of operators (PISO) scheme is employed to treat the pressure–velocity coupling. k and ε equations are coupled in the scheme and solved by a segregated approach. As for free surface simulation, a compressive interface capturing scheme for arbitrary meshes (CICSAM) is used to capture the fluid interfaces [14]. For the porous flow, an implicit method is used to solve the Forchheimer's equation [7]. The unified equation (Eq. (11)) is solved for pollutant transport in both two regions, which avoids repeated iteration on the interface boundary. For the overlying water body, the adsorbent concentration S is set to zero.

In order to ensure satisfactory precision, there are eighty grids in a wavelength in the x direction. Local re-

finement is needed in the y direction and there are at least ten grids in the region of free surface. Furthermore, the Courant number is used to obtain the dynamic time step at the beginning of each calculation cycle, defined as

$$C_n = \frac{u_i \Delta t}{\Delta x_i}, \tag{20}$$

where Δt is the time step, Δx_i represents the mesh size and the Courant number is equal to 0.1 during calculation.

The dynamic computational procedure for the present coupling model can be summarized as follows. As showed in Fig. 2, firstly, the N–S equations is explicitly solved and the velocities of wave field are obtained; secondly, the Forchheimer's equation is implicitly solved and the velocities of the porous flow are gotten; thirdly, the pressure for the total domain is adjusted to satisfy the continuity equation; fourthly, the turbulence model is solved. The turbulent kinetic energy and the turbulent energy dissipation rate are obtained; fifthly, the water–air free surface is captured by the VOF method; sixthly, the pollutant release rate and capture rate are calculated according to the velocity of the porous flow; finally, the advection-diffusion equations are solved and the distributions of adsorbent concentration and suspension concentration can be obtained.

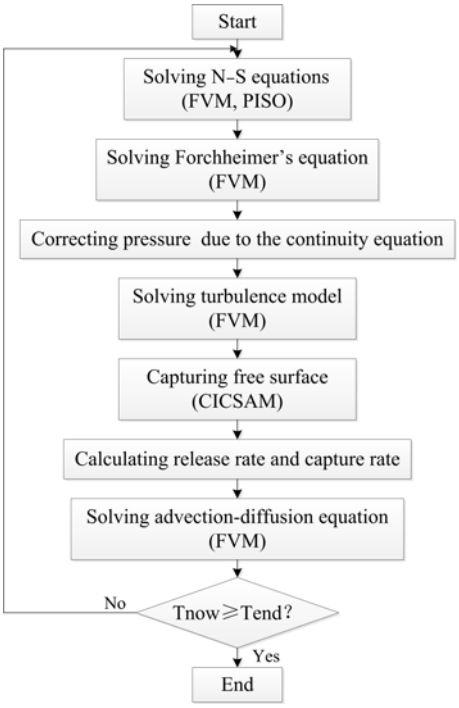

Fig. 2 Computation flow chart

It must be point out that the present computational model is a two-dimensional model, which indicates that the model is suitable for cases with flat or little fluctuated interface shape in the third (z) direction. The model can be easily extended to three-dimension model, but it needs great amount of calculation.

4 Model validation

In order to verify the coupled numerical model of wave interaction with porous medium, the distributions of wave height over permeable beds are calculated and compared with experiments. A series of experiments were performed by Sawargi and Deguchi [15], which could be used to determine the wave attenuation over permeable beds. For the selected experiment, the wave period T and wave height were 1.50 s and 0.035 8 m, respectively. The water depth d was 0.15 m. The porous bed was constructed by stones with mean diameter of 3.07 cm and the seabed thickness was 0.15 m. Figure 3 shows the comparison of the present numerical results with experimental and other numerical results. The other numerical results come from Cheng et al. [7], and Karunarathna and Lin [16]. The figure shows a good agreement between the numerical results and experimental data, which indicates that the proposed numerical model can accurately simulate the wave interaction with porous seabed.

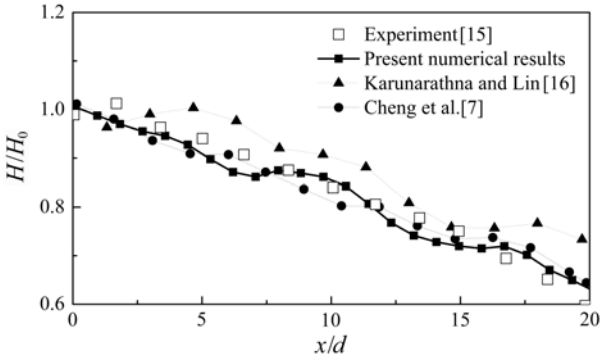

Fig. 3 Comparison of numerical results with experimental data for wave interaction with porous seabed

Next, the pore network model is applied to the problem of pollutant flowing through porous bed and the results are compared with the experiment of Baghdikian et al. [17]. The size of the network is 40×40. Two runs of the experiment are simulated and the corresponding parameters are listed in Table 2.

Table 2 Experiment parameters

Physical quantities	Run 7	Run 6
Ionic strength/(mol·L^{-1})	0	0.1
Injection rate/(cm^3·min^{-1})	8.6	8.6
H/J	3.5×10^{-20}	3.5×10^{-20}
Φ_p/mV	−70	−80
Φ_s/mV	−50	−90
pH	10.0	10.0
Concentration C_0/ppm	2×10^3	2×10^3

As showed in Fig. 4, the simulated permeability reduction due to pollutant deposition and capture are compared with the results of experiment, which turns out to fit the experiment results well.

Finally, the pollutant transport calculation is verified against an experimental case for transport of phosphorus in circulating water channel, given by Zhang [18]. The phosphorus is one of the main pollutants in coastal zones and it is the major research object in the present study. In this case, the water depth is 0.15 m, the mean velocity in channel is 0.1 m/s, the thickness of porous bed is 0.05 m, the characteristic diameter of porous bed is 0.3 mm and the porosity is 0.4. The initial phosphorus concentration in porous media is 7 mg/l. A comparison of numerical results and experimental data is shown in Fig. 5. The numerical results agree well with experimental data, which indicates that the dynamic coupling model can accurately simulate the pollutant transport.

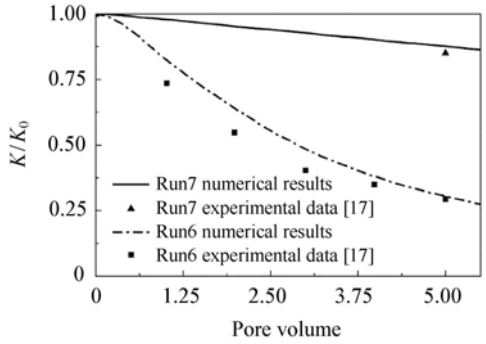

Fig. 4 Comparison of predicted relative permeability reduction with experiment

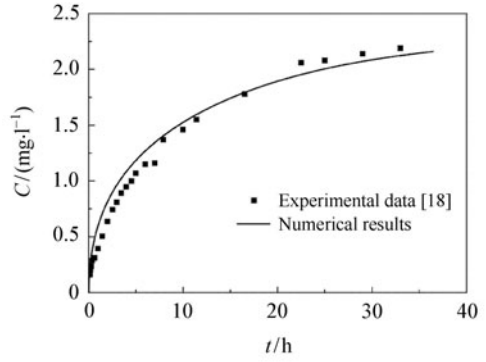

Fig. 5 Simulated phosphorus changes in the water

5 Results and analysis

5.1 Pollutant release and capture rate

Hydrodynamics condition has great impact on pollutant capture/release process. A series of simulations are carried out for different flow rates ranging from 0.02 mm/s to 1.0 mm/s, which is also approximately the range of the flow velocity in porous bed used in the following numerical cases.

The calculated release rate and capture rate are shown in Figs. 6 and 7, respectively. The pore velocity represents the flow velocity in pore space. It can be seen that both the capture and the release rates increase as the inject velocity increases. The change trend and magnitude order of calculated results are basically the same compared with the Joon's experimental data [19]. Furthermore, there exists a critical velocity of about 0.2 mm/s in pollutant release rate, which is close to the deduced value of experiment of Tripathy [20].

In order to couple these calculated rates to simulate the pollutant transport, the calculated results must be fitted firstly. The fitting curves in Figs. 6 and 7 can be expressed by a polynomial equation as

$$f(k_{r/c}) = B_0 + B_1 u + B_2 u^2 + B_3 u^3, \tag{21}$$

where, B_0, B_1, B_2, and B_3 are polynomial coefficients. The three power polynomial fitting coefficients of release rate and capture rate are listed in Table 3.

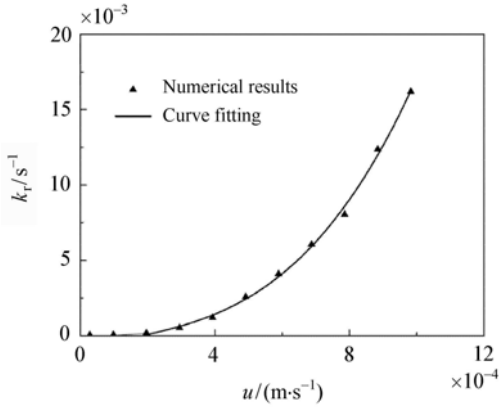

Fig. 6 Changes of k_r with pore velocity

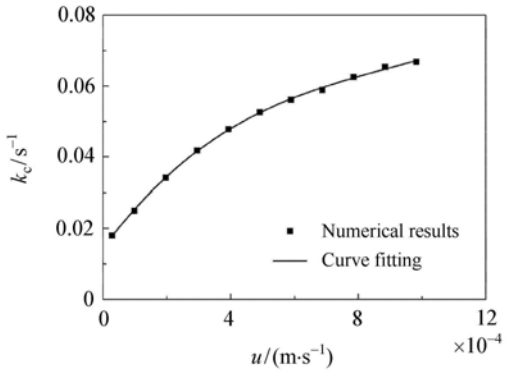

Fig. 7 Changes of k_c with pore velocity

Table 3 Polynomial fitting coefficients

Value	B_0	B_1	B_2	B_3
k_r	-8.6×10^{-4}	5.17	-6.26×10^3	1.91×10^7
k_c	0.011 5	119	-1.04×10^5	3.82×10^7

5.2 Effect of water depth

After the validation of the numerical model, the process of phosphorus transport under different water depths are investigated. Table 4 gives the input property of water depth. The value of dimensionless water depth (d/L) ranges from 0.18 to 0.43, which indicates that the incident wave belongs to limited deep-water wave and can be expressed by Stokes wave theory. The wave period T and wave height H are 3.0 s and 0.3 m, respectively. The initial adsorbent concentration in porous media (S_0) is 10 mg/L.

Table 4 Water depth inputs

Case	1	2	3
d/m	2.0	4.0	6.0
d/L	0.18	0.30	0.43

The simulations are performed for $200T$. Figure 8 shows the phosphorus concentration distribution for the second case ($d/L = 0.3$) with four different time points. From Fig. 8, it can be seen that the dimensionless concentration (C/S_0) is higher than 0.04 in porous bed at the time of $25T$. It indicates that more and more phosphorus pollutant is released from the porous media due to the increase of the pore velocity. Because of the periodic motion under wave condition, the release of the phosphorous exhibits a periodic change at the time of $50T$. The released phosphorus continually enters into the overlying water with time and the pollutant concentration in overlying water increases correspondingly.

Figure 9 shows the vertical distribution of pollutant concentration along water depth for different relative positions (h/d) at the time of $25T$. In addition, a comparison of computed results between two cross sections at $x = 4L$ and $8L$ is also illustrated. As can be seen from Fig. 9, the pollutant concentration decreases quickly with the increase of h/d, and the vertical distribution of phosphorus concentration increase with the decrease of d/L. There is a higher concentration gradient across the bed-water interface, which indicates that the porous bed plays an important role in pollutant transport.

Figure 10 shows the average suspension concentration of phosphorus in porous media and overlying water-body for different d/L. The suspension concentration represents the concentration of the pollutants in water, which indicates the amount of pollutants released from the porous media. Figure 10 shows that the released amount of pollutant decreases with the increase of the water depth and the transport velocity of pollutant decreases correspondingly. Under the same wave height and period condition, the higher the dimensionless water depth, the weaker the effects of the wave to the porous bed and the smaller the porous velocity, so the amount of pollutant released from the porous bed is lower. The average phosphorus concentration in porous media reaches peak value at the time about $24T$. And then, the suspension concentration decrease rapidly with the increase of time until reaching equilibrium. The equilibrium concentration in overlying water for $d/L = 0.18$ is 809% greater than that for $d/L = 0.43$. The suspension concentration in porous bed increases firstly and then decreases because of many reasons. The pore velocity increases rapidly with the wave propagation at the beginning stage. After the phosphorus concentration reaches the peak value, more and more phosphorus enters into the overlying water and a certain fraction of phosphorus is absorbed by porous media again. Figure 11 shows the average adsorbent concentration in porous

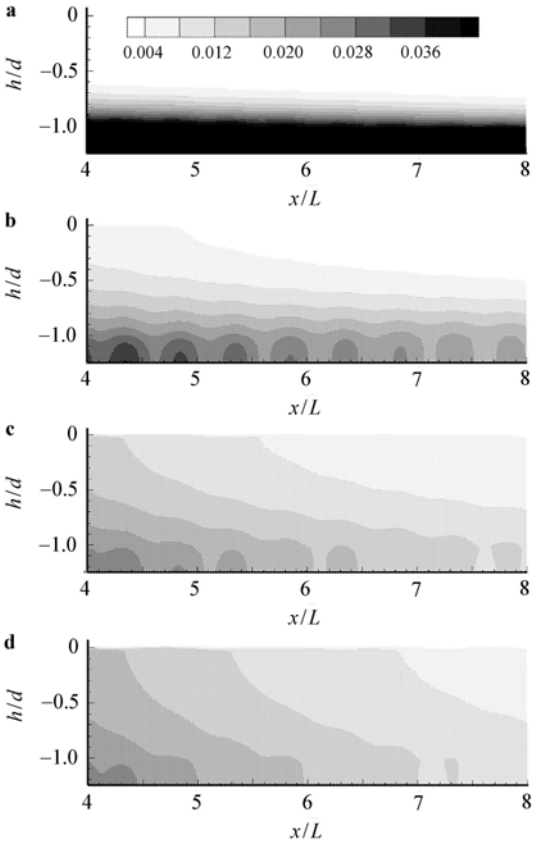

Fig. 8 Contour plots of the pollutant concentration (C/S_0). **a** $t = 25T$; **b** $t = 50T$; **c** $t = 75T$; **d** $t = 100T$

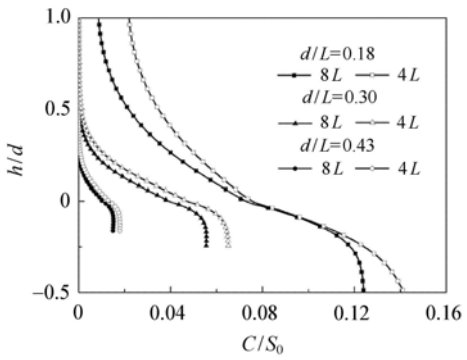

Fig. 9 Vertical distribution of pollutant concentration

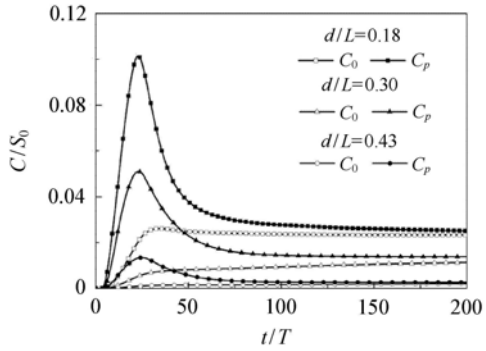

Fig. 10 Average suspension concentration in porous media and overlying water-body

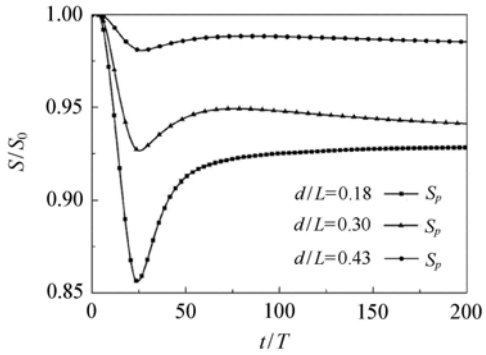

Fig. 11 Average adsorbent concentration in porous media

media. The average adsorbent concentration in porous bed for $d/L = 0.18$ is 6% lower than that for $d/L = 0.43$, which indicates that there are more phosphorus pollutant released from the porous media and entered into the water body.

5.3 Effect of incident wave height

For the purpose of investigating the effect of incident wave height on pollutant transport, totally three numerical cases are simulated for regular waves. The water depth d and period T are 4.0 m and 3.0 s, respectively. Table 5 lists the input property of wave height. The wave height ranges from 0.1 m to 0.5 m, which belongs to the normal range of wave height in China offshore.

Table 5 Incident wave height inputs

Case	1	2	3
H/m	0.1	0.3	0.5
H/d	0.025	0.075	0.125

Figure 12 illustrates the average suspension concentration of phosphorus in porous media and overlying water for different dimensionless wave height (H/d). The average pollutant concentration in porous media reaches the peak value at the time about $23T$ for the case of $H/d = 0.075$ and $H/d = 0.125$, while the concentration reaches the peak value at the time $t = 40T$ for the case of $H/d = 0.025$. Under the same wave period and water depth condition, the dimensionless wave height is lower, the flow velocity in overlying region and porous media is smaller, and the turbulence of the both regions is weaker, so the pollutant concentration reaches the peak value slower. The equilibrium concentration in overlying water for $H/d = 0.125$ is 55% greater than that for $H/d = 0.075$, and 837% greater than that for $H/d = 0.025$. The higher the dimensionless wave height, the larger the porous velocity. In this situation, there is more amount of pollutant released from the porous and the equilibrium concentration will be higher. Figure 13 shows the average adsorbent concentration in porous bed. The average adsorbent concentration in porous bed for $H/d = 0.125$ is 9% lower than that for $H/d = 0.075$, and 8% lower than that for $H/d = 0.025$. More amount of pollutant is released from the porous bed at the high H/d and the adsorbent concentration will be lower correspondingly. In general, the released amount of pollutant and the transport velocity of pollutant increase with the increase of the wave height.

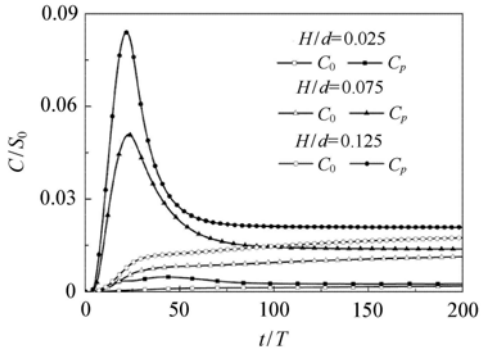

Fig. 12 Average suspension concentration in porous media and overlying water-body

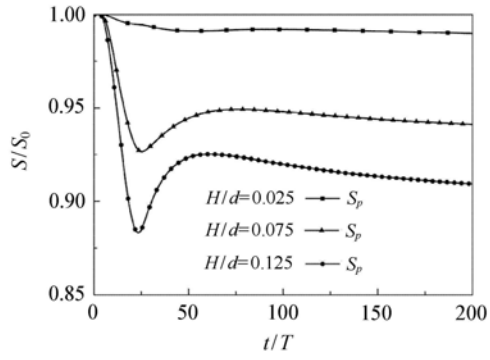

Fig. 13 Average adsorbent concentration in porous media

5.4 Effect of incident wave period

In this section, effect of incident wave period on the pollutant transport is illustrated. The water height H and water depth d are 0.3 m and 4.0 m, respectively. Table 6 gives the input property of dimensionless wave period ranging from 3.1 to

6.3, which contains variant degrees of wave nonlinearity.

Table 6 Incident wave period inputs

Case	1	2	3
T/s	2.0	3.0	4.0
$T\sqrt{g/d}$	3.1	4.7	6.3

Figure 14 shows the average suspension concentration of phosphorus in porous media and overlying water-body for different $T\sqrt{g/d}$. The average phosphorus concentration in porous media reaches the peak value at the time of $22.9T$ and $15.7T$ for the case of $T\sqrt{g/d} = 4.7$ and $T\sqrt{g/d} = 6.3$, respectively. The larger the dimensionless wave period, the stronger the nonlinearity of the wave. The values of diffusion coefficient and transfer velocity increase as the nonlinearity of the wave enhances. The average phosphorus concentration in porous media and overlying water-body for $T\sqrt{g/d} = 3.1$ is very small. In this case, $d/L = 0.63$ and the wave belongs to deep sea wave, which indicates that the wave has very little effect on the porous bed. The equilibrium concentration in overlying water for $T\sqrt{g/d} = 6.3$ is 42% greater than that for $T\sqrt{g/d} = 4.7$. The amount of the released pollutant increases as the nonlinearity of the wave enhances. Figure 15 shows the average adsorbent concentration in porous media. It can be seen that the initial adsorbent concentration in porous media is basically unreleased for the case 1. Under this condition, the pore velocities in most of the porous region are lower than critical release velocity and nearly no pollutant is released from the porous bed. The average adsorbent concentration in porous bed for case 3 is 10% lower than that for case 2. The amount of the adsorbent pollutant decreases as the nonlinearity of the wave enhances, and the released amount of pollutant increases with the increase of the wave period. The transport velocity of pollutant is high and the increment of suspension concentration is significant when the dimensionless period is relatively large.

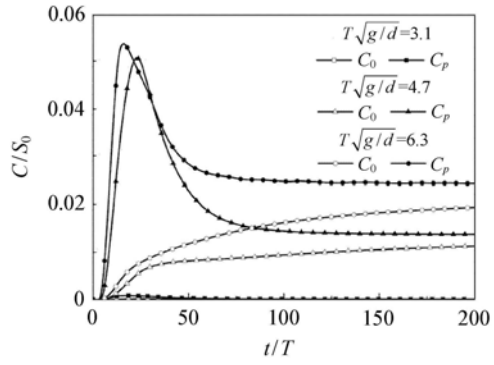

Fig. 14 Average suspension concentration in porous media and overlying water-body

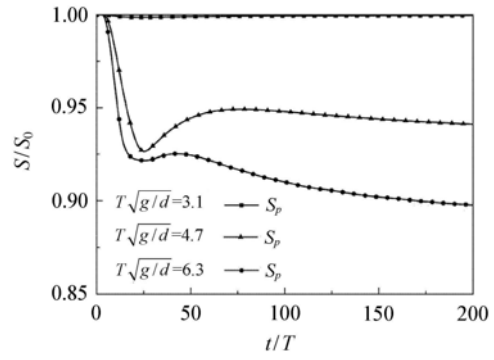

Fig. 15 Average adsorbent concentration in porous media

6 Conclusion

Wave is a common phenomenon in the ocean and it is a very important dynamic factor. In the study on pollutant transportation, the influence of wave should be considered. A dynamic coupling numerical model is proposed here, in which the coupling between wave field of overlying water-body and seepage of porous bed, the capture and release of pollutant in porous bed, and the transport process between the two different regions are taken into account.

Research shows that the water depth, wave height and wave period have great influences on the release, capture and transport processes of phosphorus pollutants. The higher the dimensionless water depth, the weaker the effects of the wave on the porous bed. The released amount of pollutant decreases with the increase of the water depth, and the transport velocity of pollutant decreases accordingly. As for the effects of wave height and wave period, in a word, the released amount of pollutant increases with the increase of the wave height and period. The higher the dimensionless wave height, the larger the flow velocity in overlying region and porous media, and the stronger the turbulence in both regions. In this situation, more amount of pollutant are released from the porous. The equilibrium concentration will be higher and the adsorbent concentration will be lower correspondingly. As for the effects of the wave period, the larger the dimensionless wave period, the stronger the nonlinearity of the wave. The released amount of pollutant increases and the amount of the adsorbent pollutant decreases as the nonlinearity of the wave enhances. Furthermore, in certain cases, the wave period is small and the wave belongs to the deep sea wave, the average phosphorus concentration will be very small.

References

1 Falconer, R.A.: Water quality simulation study of a natural harbor. Journal of Waterway, Port, Coastal, and Ocean Engineering **112**, 15–33 (1986)

2 Mestres, M.: Three-dimensional simulation of pollutant disper-

sion in coastal waters, [Ph.D Thesis]. Universitat Politècnica de Catalunya, Spanish (2002)
3 Tao, J.H., Han, G.: Effects of water wave motion on pollutant transport in shallow coastal water. Science in China (Ser. E) **45**, 593–605 (2002)
4 Sun, T., Tao, J. H.: Numerical simulation of pollutant transport acted by wave for a shallow water sea bay. International Journal for Numerical Methods in Fluids **51**, 469–487 (2006)
5 Tang, J., Shen, Y.M., Qiu, D. H.: Numerical simulation of longshore currents and pollutant movement in waves and currents in coastal zone. Acta Oceanological Sinaca **30**,145–155 (2008)
6 Tang, J., Cui, L.: Numerical study of pollutant transport in breaking random waves on mild slope zone. Procedia Environmental Sciences **2**, 274–287 (2010)
7 Cheng, Y.Z., Jiang, C.B., Wang, Y.Y.: A coupled numerical model of wave interaction with porous medium. Ocean Engineering **36**, 952–959 (2009)
8 Hsu, T.J., Sakakiyama, T., Liu, P.L.F.: A numerical model for wave motions and turbulence flows in front of a composite breakwater. Coastal Engineering **46**, 25–50 (2002).
9 Zang, J.: Wave induced seepage force action on cylinder sitting on deformable seabed, [Ph.D Thesis]. Dalian University of Technology, China (1992) (in Chinese)
10 Van Gent, M.R.A.: Porous flow through rubble-mound material. Journal of Waterway, Port, Coastal, and Ocean Engineering **121**, 176–181 (1995)
11 Compere, F., Porel, G., Delay, F.: Transport and retention of clay particles in saturated porous media. Influence of ionic strength and pore velocity. Journal of Contaminant Hydrology **49**, 1–21 (2001)
12 Khilar, K., Fogler, H.S.: Migration of Fines in Porous Media. Kluwer Academic Publishers, Netherlands (1999)
13 Vaidyanathan, R., Tien, C.: Hydrosol deposition in granular beds. Chemical Engineering Science **43**, 289–302 (1988)
14 Ubbink, O., Issa, R.I.: A method for capturing sharp fluid interfaces on arbitrary meshes. Journal of Computational Physics **153**, 26–50 (1999)
15 Sawargi, T., Deguchi, I.: Wave on permeable layers. In: Proceedings 23rd International Conference on Coastal Engineering, ASCE, Venice, 1531–1544 (1992)
16 Karunarathna, S.A., Lin, P.Z.: Numerical simulation of wave damping over porous seabeds. Coastal Engineering **53**, 845–855 (2006)
17 Baghdikian, S.Y., Sharma, M.M., Handy, L.L.: Flow of clay suspensions through porous media. SPE Reservoir Engineering **4**, 213–220 (1989)
18 Zhang, K.: Research of contaminated sediments effect on overlying water quality, [Ph.D Thesis]. Shanghai University, China (2011) (in Chinese)
19 Joon, S.Y.: Discrete particle transport in porous media: direct observations of physical mechanisms influencing particle behavior, [Ph.D Thesis]. MIT, USA (2005)
20 Tripathy, A.: Hydrodynamically and chemically induced in situ kaolin particle release from porous media an experimental study. Advanced Powder Technology **21**, 564–572 (2010)